STANFORD GEOTHERMAL PROGRAM

QUARTERLY REPORT

JANUARY 1 - MARCH 31, 1997

1 AN EXPERIMENTAL STUDY OF BOILING IN POROUS MEDIA

This research project is being conducted by Dr. Cengiz Satik. The objective of this study is to improve our understanding of the process of boiling in porous media by using both experimental and numerical methods.

1.1 SUMMARY

The ultimate goal of this study is to understand the origin of the two important but currently unknown functions of relative permeability and capillary pressure functions. In earlier quarters we conducted a series of experiments, but determined that the pressure measurements being made were of insufficient accuracy. During the current quarter, an attempt was made to conduct a vertical boiling experiment using a Berea sandstone core sample with an improved pressure measurement system. However, the experiment had to be terminated due to excessive leaks. These will be discussed in this report.

1.2 INTRODUCTION

The process of boiling in porous media is of significance in geothermal systems as well as in many other applications such as porous heat pipes, drying and nuclear waste disposal. Despite its importance, the fundamentals of this process are poorly understood. Most of the problems arise from the lack of the understanding of the mechanics and dynamics of this complex process.

A look at the previous literature shows that many attempts have been made in both experimental and theoretical directions to investigate and to describe the process of boiling in porous media (Satik, 1994). Most previous studies have used continuum formulations which made use of Darcy's law extended to multiphase flow with relative permeability and capillary pressure functions derived from isothermal gas-liquid displacement processes. These processes have major differences to boiling displacement which involves additional phenomena such as heat transfer, nucleation and phase change. Moreover, the continuum approaches are also limited by the assumption of capillary control at the pore level (low Capillary and Bond numbers). Due to these restrictions and uncertainties, it is unclear whether the relative permeability and capillary pressure functions currently used for modeling the process of boiling in porous media are appropriate. At the same time, fundamental studies focusing at the microscopic pore scale have been very limited. In a recent study by Satik and Yortsos (1996), numerical and experimental pore networks were used to model boiling in porous media at a microscopic scale. Satik and Yortsos (1996) developed a numerical pore network model for boiling in a horizontal, two-dimensional porous medium and conducted visualization experiments by using glass micromodels. Although progress was made, their model was developed only for a single bubble growth in a horizontal porous medium, ignoring the effects of gravity. Therefore, further work is still needed to improve the understanding and to resolve the issues raised by the continuum formulations (see Satik, 1994, for details) and eventually to obtain correct forms of the relative permeability and capillary pressure functions.

In this work, we used a different technique to study this problem. We conducted experiments with real core samples such as from Berea sandstone. Using an X-ray computer tomography (CT) scanner, we visualized the process and determined the three-dimensional fluid distributions within the core while the experiment was in progress. By using thermocouples, pressure transducers and heat flux sensors under the control of a data-acquisition computer, we obtained temperature, pressure and heat flux values along the core. The comparison of the experimental data with the results of a numerical simulator will give us an opportunity to check the results. Using an optimization tool that matches a numerical simulation to the experimental results, the appropriate form of the relative permeability and capillary pressure functions will be obtained. Finally, our ultimate goal is to be able to carry out these experiments with core samples obtained from The Geysers geothermal field.

1.3 RESULTS

A schematic of the experimental apparatus and procedure were shown in the previous quarterly report. Briefly, the apparatus consists of a core holder, a data acquisition system, a vacuum pump, a liquid pump and a balance. Ten pressure taps and thermocouples are placed along the core length to measure pressures and temperatures. A heater and a heat flux sensor are placed in the specially designed inlet end of the core holder. In addition, several heat flux sensors are placed along the core to measure heat losses. During an experiment, the core holder is placed inside the high resolution X-ray CT equipment to obtain *in-situ* saturation profiles along the core (Satik, 1997).

Two experiments were conducted during the last quarter of 1996 and the results were presented at the 1997 Stanford Reservoir Engineering Workshop (see Satik, 1997 for details). The results of the two experiments indicated the need for a better pressure measurement system. Therefore, during the last quarter, the pressure measurement system was improved by acquiring a new set of pressure transducers and another attempt was made to conduct a vertical boiling experiment using a Berea sandstone core sample. Although this experiment had to be terminated due to leaks from the core, we were able to collect partial data. Histories of measured heat flux at the heater and temperatures are shown in Figures 1.1 and 1.2 respectively. Preparation of a new core for a future experiment is currently in progress. Also a further modification to the core holder that would allow both vertical and horizontal boiling experiments with the same core is under consideration. Upon completion of these modifications, we will conduct another experiment during the coming quarter.
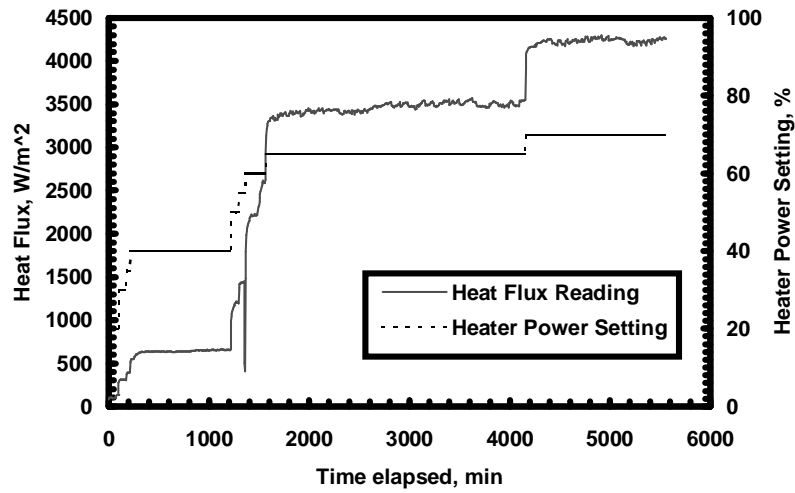
Figure 1.1: Heater power settings and corresponding heat flux values obtained from the heat flux sensor.
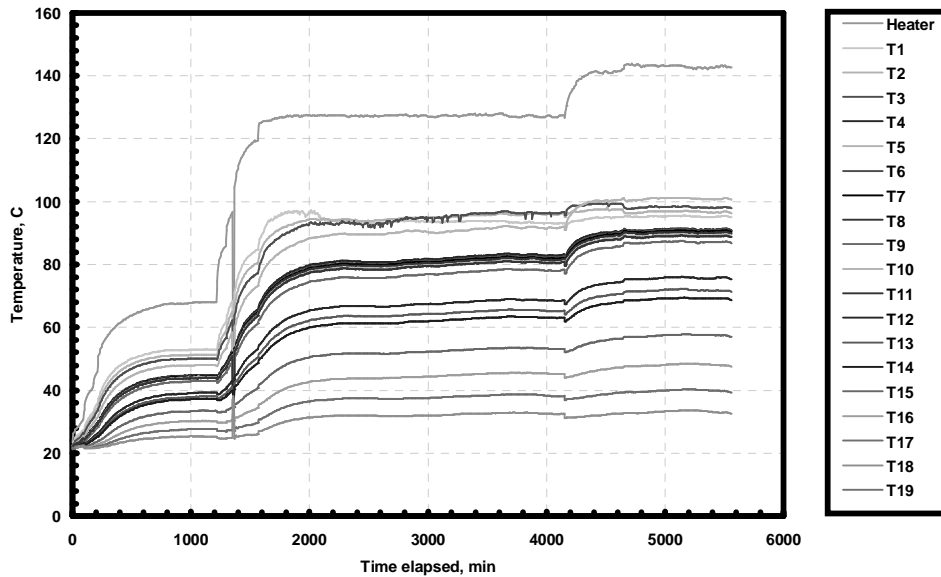

Figure 1.2: Histories of 19 wall temperatures and heater temperature during the vertical boiling experiment.

2   MEASUREMENTS OF STEAM-WATER RELATIVE PERMEABILITY

This project is being conducted by Research Assistant Raul Tovar, Dr. Cengiz Satik and Professor Roland Horne. The aim of this project is to measure relative permeability relations for steam and water flowing simultaneously in a porous medium.

2.1 SUMMARY

A measurement of relative permeability relations for simultaneous flow of steam and water in porous media was attempted in steady state experiments conducted under conditions that eliminate most errors associated with saturation and pressure dtermination. However, sufficient power to obtain superheated steam could not be achieved at the steam inlet of the core. This made it difficult to measure the fluid enthalpy as it was in the two-phase zone. Therefore a new injection system was designed as described in the following section. Subsequent experiments showed the expected behavior with the new design until the core failed.

2.2 EXPERIMENTAL APPARATUS AND PROCEDURE

Previously, the experimental apparatus consisted of an injection unit with two furnaces to generate steam and hot water as described in the previous report. However, the steam generator did not supply sufficient heat to produce superheated steam. Therefore the design was changed to a system with only a single injection unit as shown in Figure 2.1. The apparatus consisted of one power controller with an ammeter used to control the heat supplied by the steam generator. Heat losses along the core body were measured by eight heat flux sensors. Temperatures were measured by eleven thermocouples, three of which were J-type thermocouples, placed along the injection, and sink lines. The remaining eight T-type thermocouples and the eight heat flux sensors were placed at equal intervals along the core body. Pressures were measured by using eleven pressure taps placed next to the thermocouples.

The proportional voltage signals from the heat flux sensors, thermocouples and pressure transducers were conditioned and collected by a data acquisition system. The data was then analyzed in a personal computer using "LABVIEW", a graphical programming software.

The Berea sandstone cores used for these experiments were 43.18 cm in length and 5.08 cm in diameter. During the preparation of a core assemblies, the core samples were first heated to $450°C$ for twelve hours to deactivate clays and to get rid of residual water. Eight ports to measure temperatures and pressures were fitted at set intervals along the edge of the core before the rest of the core was covered completely by high temperature epoxy. The core was tested for leaks before being covered with an insulation made of ceramic blanket. Experiments were conducted inside a high resolution X-ray CT scanner so that in-situ saturations could be measured, while the experiment was in progress.
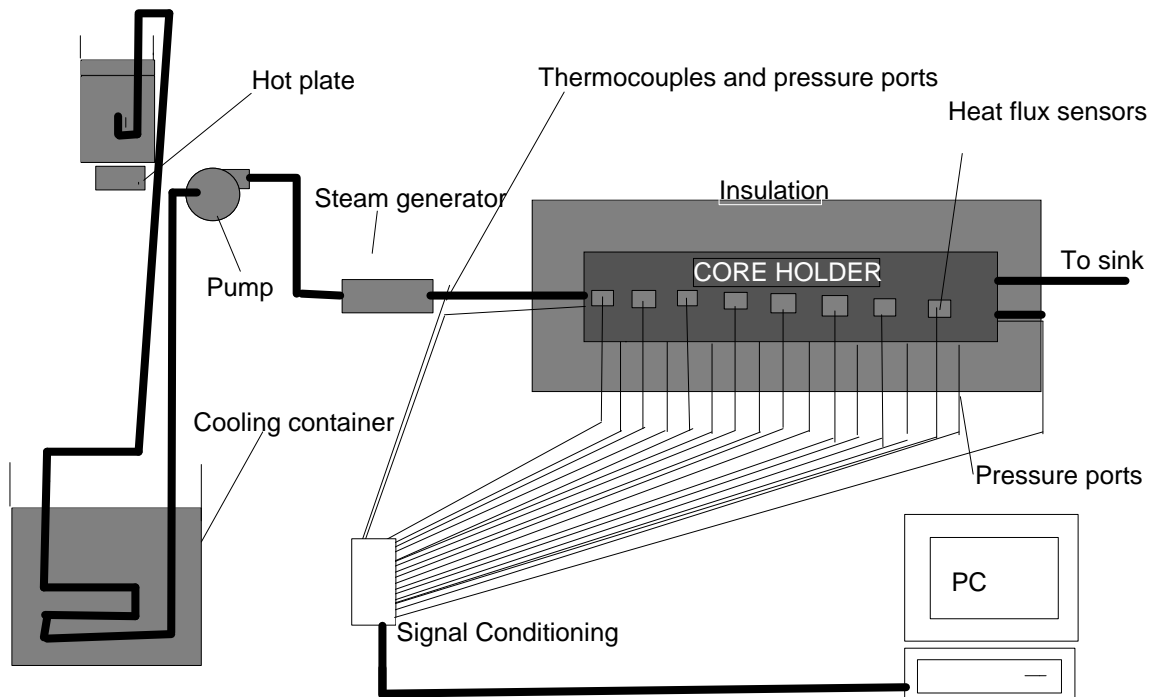
Figure 2.1 Experimental apparatus.

and thermocouples

Air initially dissolved in the water would give erroneous saturation readings, so was removed by boiling and cooling the water before injecting into the core as shown in Figure 2.1. Also, the core was evacuated beforehand to remove air trapped inside the pore space.

During the experiment, the power of the steam generator was increased in steady state steps. That is, the power was not increased to the next step until steady conditions had been reached. Initially the water was at sub-cooled conditions and was slowly brought up to the saturation line. Then the power was raised in steps through the saturation zone until the steam saturation line was reached. This procedure allows the calculation of the fluid flowing fraction as described below.

2.3 CALCULATIONS

Water temperature increases linearly as heat is supplied until the two phase zone is reached. Once in the two phase zone the water temperature no longer changes. However the steam quality increases from zero to one as the heat supplied is increased. At the vapor saturation line the steam quality reaches its maximum and, once again, the fluid temperature increases linearly with respect to the supplied heat. This method assumes constant heat transfer rate from the steam generator to the fluid and constant heat losses through the lines in the saturated zone. This allows us to divide the saturation dome proportionally to the heat supplied by the steam generator at each step to obtain the steam mass flowing fractions x as follows:

6

$$power = c + mx \tag{2.1}$$

where c and m are constants. Then, solving for x we obtain:

$$x = \frac{amps - c}{m} \tag{2.2}$$

The constants are evaluated at the saturated liquid line and at the saturated vapor line. Then the relative permeabilities to steam and water can be calculated by the corresponding Darcy equations for each phase in terms of the mass flow rates

$$k_{rl} = -\frac{(1-x)m_t \mu_l \nu_l}{kA\frac{\Delta p}{\Delta x}} \tag{2.3}$$

and

$$k_{rs} = -\frac{xm_t \mu_s \nu_s}{kA\frac{\Delta p}{\Delta x}} \tag{2.4}$$

2.4 PRELIMINARY RESULTS

Figure 2.2 shows the temperature variation at the core inlet as a function of heat supplied. The plot eventually flattens at about 300 watts meaning the onset of two phase flow (saturated liquid). The peak at about 430 watts could be wrongfully interpreted as the onset of saturated vapor. However, Figure 2.3 shows a peak in the core inlet pressure at the same power setting implying that the fluid was still in the two phase zone. After the peak the water temperature remains fairly constant up to the end of the experimental data.
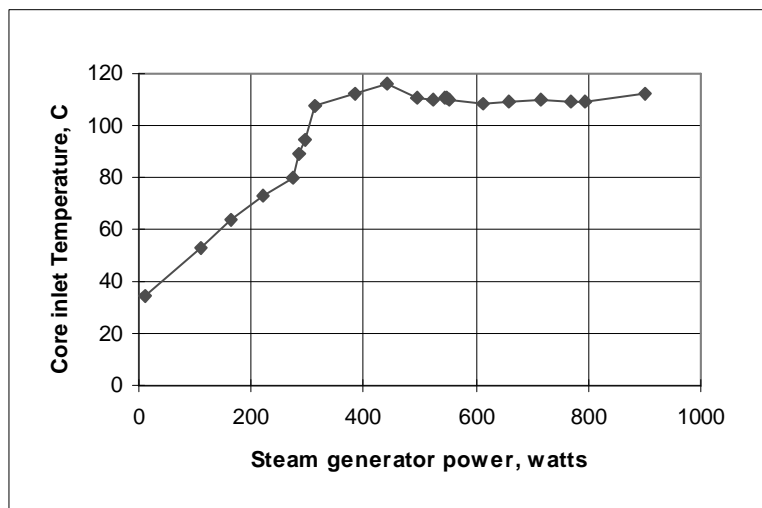

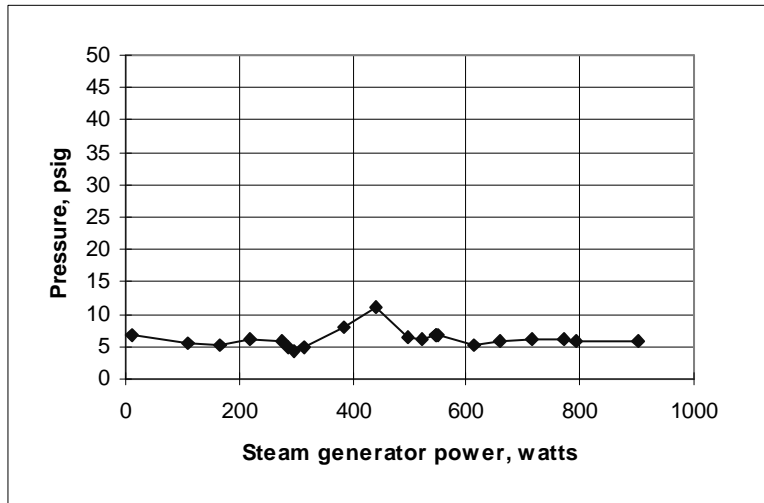*Figure 2.2 Water temperature versus heat supplied.*

Figure 2.3 Water pressure versus heat supplied.

2.5 CONCLUSION

The experiments in the current quarter revealed only partial results as the core failed before superheated conditions could be reached. Note the small pressure variation throughout the experiment shown by Figure 2.3. In view of this partial agreement between theory and the experimental data, Equation (2.3) is believed to be an adequate estimate of the steam flowing fraction.

3 BOILING IN POROUS MEDIA

This research project is being conducted by Research Assistant Marilou Guerrero, Dr. Cengiz Satik, and Prof. Roland Horne. The objective of this study is to simulate results obtained from the vertical boiling experiment described in Section 1 using the commercial simulator, TOUGH2. This is done to give us a better understanding of boiling in porous media, and to ultimately formulate the appropriate relative permeability and capillary pressure functions in steam-water systems.

3.1 SUMMARY

The first objective of this study is to simulate the boiling process in the vertical core experiment detailed in Satik (1997). During the current quarter, numerical results using combinations of known relative permeability and capillary pressure functions were compared with the experimental measurements. However, none of the numerical simulations exactly mimic the temperature, pressure, and steam saturation measurements obtained from the experiments. This is probably be due to the fact that the relative permeability and capillary functions used in the simulations are not applicable to the steam-water flows in the experiments.

3.2 NUMERICAL SIMULATION

In the actual experiment, the 43-cm long Berea sandstone core of radius 25 cm, was covered with epoxy. It was saturated with liquid water, after which a heater was attached to the bottom. The top end was maintained at atmospheric pressure.

In the TOUGH2 simulation runs, the core was divided into six rings and ten layers, giving a total of 60 grid blocks. Heat is applied to the bottom layer, while a constant pressure boundary is ensured on the top layer by specifying a very large volume. The thermal conductivity, absolute permeability, and porosity of the sixth ring (outermost ring) were set to be infinitesimally small to ensure no fluid flow and no heat transfer through and within the sixth ring.

3.3 RESULTS AND DISCUSSION

The two relative permeability functions used in the simulation runs were the linear and Sandia functions. For the linear function, the liquid relative permeability, k_{rl} increases linearly from 0 to 1 in the range $0.2 \leq S_l \leq 1$. Similarly, the gas relative permeability, k_{rg} increases linearly from 0 to 1 in the range $-1 \leq S_l \leq 0$. For the Sandia function, the liquid and gas relative permeability functions are given by:

$$k_{rl} = \begin{cases} \sqrt{S^*} \left\{ 1 - (1 - [S^*]^{1/\lambda})^\lambda \right\}^2 \ if \ S_l \prec S_{ls} \\ 1 \ if \ S_l \geq S_{ls} \end{cases} \qquad (3.1)$$

$$k_{rg} = 1 - k_{rl} \qquad (3.2)$$

9

where

$$S^* = (S_l - S_{lr}) / (S_{ls} - S_{lr}),$$ (3.3)

and S_l is the liquid saturation, S_{lr} is the residual liquid saturation, and λ is the mobility ratio.

The two capillary pressure functions used in the simulations runs were the linear and Sandia capillary pressure functions. For the linear function,

$$P_{cap} = \begin{cases} -CP(1) \; for \; S_l \leq CP(2) \\ 0 \; for \; S_l \geq CP(3) \\ -CP(1).\dfrac{CP(3)-S_l}{CP(3)-CP(2)} \; for \; CP(2) \prec S_l \prec CP(3) \end{cases}$$ (3.4)

for $CP(3) > CP(2)$.

For the Sandia function, capillary pressure is given by

$$P_{cap} = \begin{cases} 0 \; if \; S_l \geq S_{ls} \\ -P_o \left\{ [S^*]^{-1/\lambda} - 1 \right\}^{1-\lambda} \\ -P_{max} \; (if \; P_o \left\{ [S^*]^{-1/\lambda} \geq P_{max} \right) \end{cases}$$ (3.5)

The results obtained from the experiment and numerical simulation were compared on the basis of pressure, temperature, and steam saturation along the length of the core. Figure 3.1 shows a comparison of pressure behavior from the bottom layer to the top layer of the core. The first group of data points is for the linear relative permeability function and Sandia capillary pressure function combination. The second set of data points is for the Sandia relative permeability and capillary pressure functions combination. The third data set is for the linear relative permeability and capillary pressure functions combination. The fourth group of data points is taken from the boiling experiment itself. As shown in Figure 3.1, although the general pressure trend is the same, i.e. it is decreasing and approaching atmospheric conditions, the simulated pressures do not quite mimic the measurements obtained from the laboratory. The closest curve to the experimental plot is the one using linear relative permeability and capillary pressure functions.

Likewise, the numerical results in terms of temperature do not have the same trend as those measured from the experiment. The temperature using linear permeability and capillary pressure functions reaches values even greater than the critical temperature of water, which is not physically possible.

Furthermore, the simulated steam saturation values do not look like the measured values. In fact, only the results obtained using the linear functions yield a curve that starts from a maximum steam saturation of 1.0 and ends at a minimum steam saturation of 0.0.

However, this response still does not mimic the boiling process observed in the experiment.
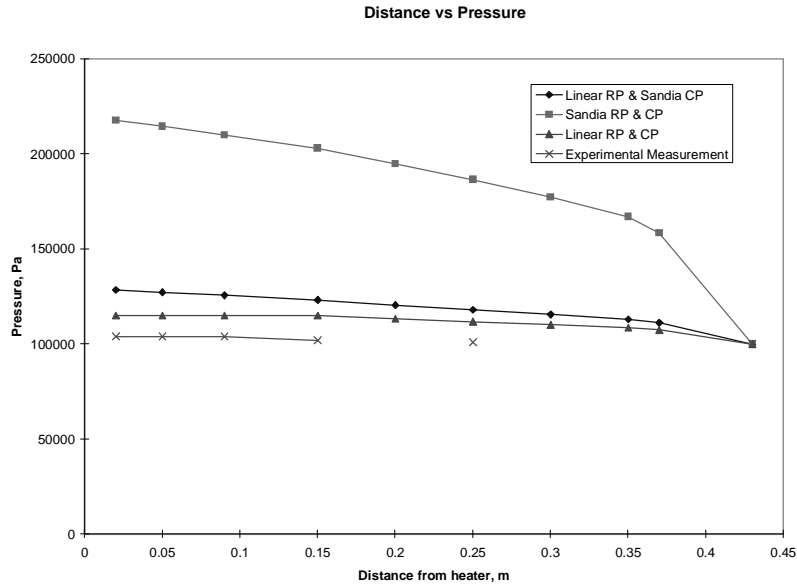
Distance vs Pressure

Figure 3.1. Pressure behavior along the length of the core.

Distance vs Temperature
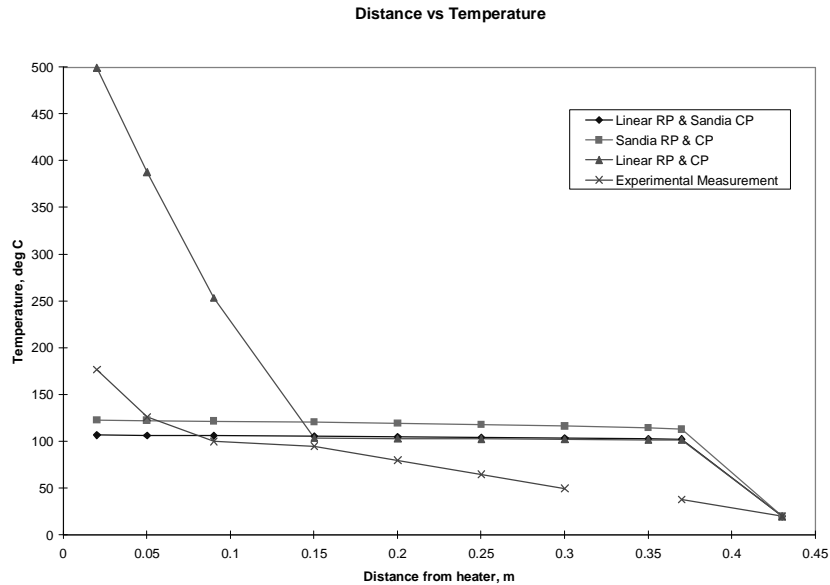
Figure 3.2. Temperature trend along the length of the core.
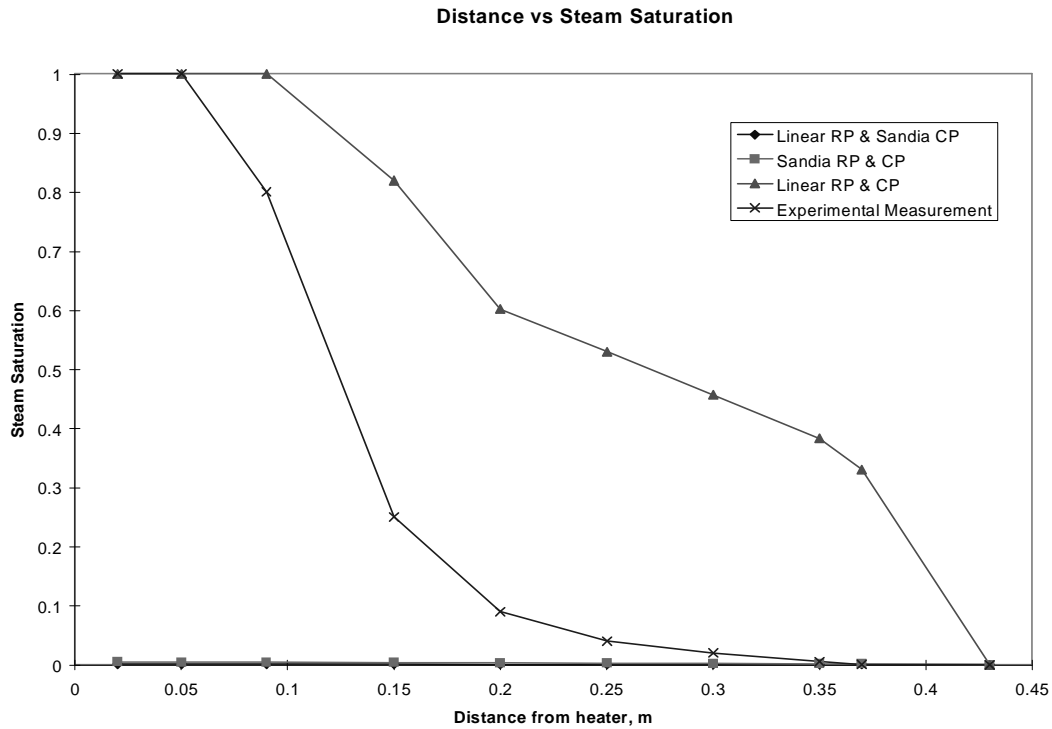
11

Distance vs Steam Saturation

Figure 3.3. Steam saturation trend along the length of the core.

3.4 FUTURE PLANS

History matching will be done by using ITOUGH2, a version of TOUGH2 that allows for the automatic variation of decision variables (such as relative permeability) in order to replicate an observed response. The results will be used to infer the appropriate relative permeability and capillary pressure functions for steam-water flow.

4 APPLICATION OF X-RAY CT SCANNING IN SATURATION AND POROSITY MEASUREMENT

This project is being conducted by Research Assistant Meiqing He, Dr. Cengiz Satik and Professor Roland Horne. The aim of this project is to identify and to characterize fractures in geothermal rocks by using X-ray computer tomography (CT). In the last quarterly report we discussed some fundamental physics in CT technique, here we will give a further brief review related to our measurement purpose, also analyze some problems existing in conducting the CT scans.

4.1 CT TECHNIQUE

The total attenuation coefficient can be represented as

$$\mu = \mu_R + \mu_P + \mu_C \tag{4.1}$$

where R, P, and C refer to Rayleigh (coherent) scattering, photoelectric effect and Compton scattering, respectively. For a composite material, these elements take the form

$$\mu = \rho N_g \left\{ f(\varepsilon) + C_R \frac{\overline{Z}_r^k}{\varepsilon^l} + C_P \frac{\overline{Z}_p^m}{\varepsilon^l} \right\} \tag{4.2}$$

where ε is the photon energy in kev, N_g is the electron mass density in electron per gram as given by

$$N_g = N_A \sum_i w_i \frac{Z_i}{A_i} \tag{4.3}$$

w_i is the proportion by weight of the ith constituent, and $\overline{Z}_r$ and $\overline{Z}_p$ are the effective atomic number as given by

$$\overline{Z}_r = \left(\sum_i \alpha_i Z_i^k \right)^{1/k} \tag{4.4}$$

$$\overline{Z}_p = \left(\sum_i \alpha_i Z_i^m \right)^{1/m} \tag{4.5}$$

In Equation (4.4) and (4.5) k, m, l, and n are exponents determined empirically, and α_i is the electron fraction of the ith element given by

$$\alpha_i = \frac{N_{gi}}{\sum_i N_{gi}} = \frac{N_A w_i \left(Z_i / A_i \right)}{\sum_i N_{gi}} \tag{4.6}$$

A_i is the atomic mass of ith constituents, and N_A is the Avagadro's number.

The Compton scattering function $f(\varepsilon)$, which is independent of the atomic number, can be described by Klein-Nishina function (Macovsky, 1983):

$$f_{kn}(\alpha) = \frac{1+\alpha}{\alpha^2}\left[\frac{2(1+\alpha)}{1+2\alpha} - \frac{1}{\alpha}\ln(1+2\alpha)\right] + \frac{1}{2\alpha}\ln(1+2\alpha) - \frac{1+3\alpha}{(1+2\alpha)^2} \qquad (4.7)$$

$$\alpha = \varepsilon / 510.975 kev \qquad (4.8)$$

These equations provide us a way to identify the material within the porous medium. As we can see from Eqn. (4.2), the attenuation coefficient is linearly dependent on the density of material, from Eqn (4.8), it depends on energy level in a nonlinear way. Those two relations combined allow us to obtain saturation and porosity by solving a set of independent equations, using measurements from scans at multiple energy levels.

4.2 APPROACHES TO POROSITY AND SATURATION MEASUREMENT

Conventionally porosity and saturation are obtained from CT measurements after saturating the porous medium with contrast agents. Water and air are most commonly used. There are two sets of CT scans needed to calculate porosity. One is the dry scan (CT_{dry}), which is conducted when the porous medium is fully saturated with air; the other is the wet scan (CT_{wet}), which is conducted after the porous medium has been saturated with water. Then the porosity is obtained by

$$\phi = \frac{CT_{wet} - CT_{dry}}{CT_{water} - CT_{air}} \qquad (4.9)$$

To calculate saturation another scan ($CT_{p_1 p_2}$) is required, which is performed when two phases, p_1 and p_2, are coexisting in the porous medium. Saturation is given by

$$S_{p_1} = \frac{CT_{p_1 p_2} - CT_{p_2 r}}{CT_{p_1 r} - CT_{p_2 r}} \qquad (4.10)$$

$$S_{p_2} = 1 - S_{p_1} \qquad (4.11)$$

where r refers to rock.

In such a measuring process, it is necessary to make sure that the core is fully saturated with contrast agent, which usually requires a long flow time.

Another approach is to use a dual energy scan technique. In this technique, two shots at two different energy levels are taken at the same slice of the core. In general, the CT number of a porous medium is in a portion weight form as below (Akin, *et al*. 1996)

$$CT = (1-\phi)CT_{Matrix} + S_{p_1}\phi CT_{p_1} + (1-S_{p_1})\phi CT_{p_2} \qquad (4.12)$$

Two sets of linearly independent data measured at two energy levels E1 and E2, CT^1 and CT^2, are substituted into Eqn. (4.12). Therefore we have

$$CT^1 = (1-\phi)CT^1_{Matrix} + S_{p_1}\phi CT^1_{p_1} + (1-S_{p_1})\phi CT^1_{p_2} \qquad (4.13)$$

$$CT^2 = (1-\phi)CT^2_{Matrix} + S_{p_1}\phi CT^2_{p_1} + (1-S_{p_1})\phi CT^2_{p_2} \qquad (4.14)$$

We can solve for porosity and saturation from the linearly independent equations. This is simpler to apply, but the key point here is how to obtain matrix CT number. One way to do this, for a homogeneous core, is to use preliminary knowledge of porosity obtained from other measurement to calculated an average matrix CT number. Substituting this estimate back into Equations (4.13) and (4.14) yields a corrected porosity value.

4.3 PRELIMINARY RESULTS

As we noticed, in both approaches discussed above, single phase CT number calibration is very important for porosity calculation. Usually, water and air are chosen as saturating agents, but their CT numbers are not always at 0 and -1000. The CT number of the single phase needs to calibrated under each scan scheme. The variation may be caused by different parameters chosen in the scan, such as energy level.

We have performed a calibration experiment by scanning a tube 1/16 inch in diameter filled with water, dry steam and nitrogen. The CT numbers of pure water and dry steam measured as a function of energy level are listed in Table 4.1.

Table 4.1: CT Number measured

	140 kev	120 kev	100 kev
Water	-124.7	-141.8	-147.1
dry steam	-960.0	-966.2	-950.3
nitrogen	-937.4	-877.6	-927.7

4.4 FUTURE WORK

We will use Berea sandstone and Geysers core to verify the two approaches discussed. In particular we will introduce heterogeneity into the matrix CT number to evaluate porosity in heterogeneous porous medium.

5 BOILING IN A VERTICAL FRACTURE ; THERMAL FRONT PROPAGATION

This project is being conducted by Research Assistant Robert DuTeaux, Dr. Cengiz Satik and Prof. Roland N. Horne. The goal of this project is to optimize strategies for injection into fractured geothermal reservoirs.

5.1 INTRODUCTION

The aims of this research have been divided into short-term, mid-term, and long-term goals. The long-term objective has been to develop a strategy for the optimization of injection into two-phase fractured geothermal reservoirs. The mid-term goal has been to either develop or employ appropriate numerical simulations to work toward the optimization goal, and the short-term work has been to begin with an experimental apparatus to observe data that can be later compared with numerical work. The effort over this past quarter has been devoted mostly to the development of experimental work with minor amounts of numerical simulation and consideration of optimization.

Some of the most significant unknowns in attempting to model fractured reservoirs has been the uncertain orientations, distributions, and permeability of fractures, however, the advancing technologies of electric logs and their interpretation as demonstrated by Barton et. al. (1997), have shown promise for better understanding of these unknowns. More accurate descriptions of the geometry of fractured systems may soon be developed with improved geophysical investigation technologies.

5.2 THE LONG TERM

5.2.1 Background

Many efforts and strategies for calculating the propagation of the thermal front away from an injection well have been conducted, and a few have employed models of discrete fractures. Notable among these have been the efforts of Gringarten et al. (1986), Bodvarsson et al. (1983 and 1985), and Pruess (1983). The simplest calculation for the thermal front in a discrete fracture with one-dimensional conduction in the direction perpendicular to flow (parallel plates of infinite thickness) was published by Carslaw and Jaeger in 1959. This model provides an extremely conservative estimate of the fastest possible propagation of a thermal front (of single phase liquid). The semianalytic works of Gringarten et al. (1986) and Bodvarsson et al. (1983 and 1985) also assume one-dimensional conduction normal to the direction of fluid propagation but extend the concept of flow in discrete fractures to multiple parallel fractures. These models have been useful for understanding that the propagation of a thermal front in low conductivity rock is very sensitive to both flow rate and fracture spacing. Only numerical simulation, however, has allowed modeling of two-phase flow and more complicated reservoir flow geometries.

5.2.2 Optimization strategy

Recognizing that the enthalpy of a geothermal fluid is the best measure of its economic value, to optimize the enthalpy of the production fluid over a chosen time period has been determined a strategy for optimal injection. This suggests for single phase flow the injected fluid must maximize the enthalpy of the production fluid over the chosen optimization interval, and for two-phase flow the injected liquid must maximize the enthalpy of steam produced. The most direct reason for simulating injection into a steam dominated system is to avoid the breakthrough of liquid in a well where pure steam has historically been produced.

The idea of tracking the movement of a thermal front along a fracture has led to the design of the experimental assembly built last quarter. In concept, a system of multiple fractures of irregular geometry and orientation can be reduced to a system with an average fracture spacing. This idea is similar to a concept developed by Robinson and Kruger (1992), and the models noted above consisting of multiple parallel fractures. With the idea of mean fracture spacing, the flow in a single fracture has been associated with the dimensions and heat capacity of a finite volume of rock. The experimental apparatus in Figure 5.1 translates the idea of a mean fracture dimension into the radial dimension of a solid cylinder of rock bounded by a flowing fracture.

5.3 EXPERIMENTAL RESEARCH

5.3.1 Description

Figure 5.1 shows the experimental assembly built in this past quarter. It was designed to measure the temperature contours and observe the propagation of a two-phase (boiling) front as the initially heated core is cooled by flow through its artificial fracture. In this configuration gravity acts as a stabilizing influence.

Because the core of the apparatus is removable, the fundamental experiment planned is to heat the core in an oven, place it in the assembly, and then inject water at saturated conditions. As the saturated water boils in the annulus, heat is transferred from the core and thermocouples measure the temperatures and monitor the propagation of the interface between the liquid and vapor. The data collected can then be used for a later verification of a numerical simulation.

5.4 NUMERICAL SIMULATION

5.4.1 Design evaluation

A single phase (liquid only) simulation was conducted to assist in the design for the placement of thermocouples in the apparatus. At a relatively low flow rate a high temperature gradient developed adjacent to the simulated fracture as illustrated by the temperature contours in Figure 5.2. This suggested that the thermocouples be placed in relatively short incremented distances away from the surface of the glass tube.
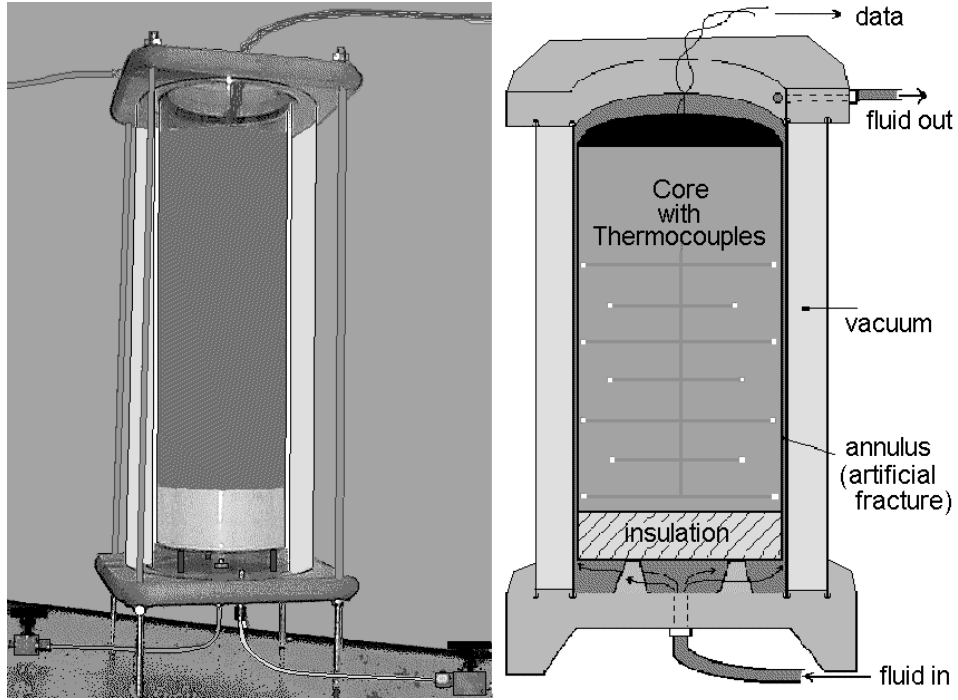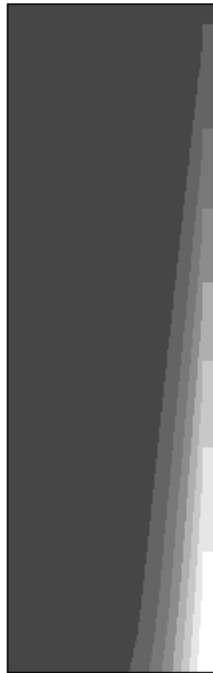
Figure 5.1 Experimental configuration.

Fig. 5.2 Simulated temperature contours

5.4.2 Continuing simulations

It was decided that future numerical investigations will be conducted with the available dual permeability and two-phase simulators with their parameters adjusted to simulate

flow in a fracture where the matrix permeability is set at a very small value. The evaluation of such models should then lead to a decision of whether or not the currently available simulators should be used for an optimization study.

6 NUMERICAL AND EXPERIMENTAL INVESTIGATIONS OF HEAT PIPES IN FRACTURED RESERVOIRS

This study is currently being undertaken by Research Assistant Nemesto Noel A. Urmeneta and Prof. Roland Horne. It was reported in the last quarterly report that the two-dimensional grid model was run to steady state for several cases using the nine-point differencing scheme. Having assigned different capillary pressure curves for the matrix and the fracture blocks, the effects of capillary pressure on the state of the system were noted.

6.1 CURRENT STATUS

The question of which differencing scheme, the nine-point or the five-point, is appropriate to the system being studied was brought up. This issue can be settled by comparing the results of the simulation runs with experimental data from a heat pipe experiment conducted by Catherine Wang and Dr. Shaun Fitzgerald. The heat pipe was constructed using a combustion tube (3 inches in diameter). It was filled up to the 1 m mark with silica sand. The top of the tube had a constant pressure, constant temperature boundary condition which was attained by connecting the tube to a water reservoir at 15°C. The bottom of the tube was subjected to a known heat flux. A series of thermocouples were positioned at the center of the tube in order to monitor the temperature with time. A numerical model was made to duplicate the experimental setup. However, numerical difficulties were encountered. This problem is still being resolved as of the moment and hence the issue of which differencing scheme to use still remains to be settled.

Regarding capillary pressures, these values are being obtained from adsorption/desorption isotherms via the Kelvin equation (Sta. Maria and Pingol, 1996)

$$p_c = \frac{RT\rho_l}{M_w} \ln\left(\frac{p_{sat}}{p_v}\right) \tag{6.1}$$

where

p_c = capillary pressure

R = universal gas constant

T = absolute temperature

M_w = water molecular weight

ρ_l = water density

p_{sat} = equilibrium vapor pressure

p_v = lowered vapor pressure

The relationship between the mass adsorbed and saturation is given by the following equation:

$$S_l = \frac{1 - \phi}{\phi} \frac{\rho_r}{\rho_l} X \qquad (6.2)$$

where

S_l = water saturation

ϕ = matrix porosity

ρ_r = rock grain density

X = mass adsorbed

Hence from an adsorption isotherm one can calculate the corresponding relationship between capillary pressure and saturation. Based on a typical Geysers adsorption isotherm, Sta. Maria and Pingol (1996) were able to obtain capillary pressures that ranged from 0 MPa to about 586 MPa (85,000 psia). Melrose (1991) on the other hand, made use of measurements from three different techniques - porous plate, water vapor desoprtion (WVD), low temperature gas desorption/adsorption and mercury injection. When the data was scaled to air/brine conditions a capillary pressure of up to 69 MPa (10,000 psia) was obtained. These two studies give us a range of possible capillary pressure values to be used in the simulation runs.

A 20 x 11 x 1 model was utilized in the simulation runs. This time, a five-point differencing scheme but the same capillary functions were used. As can be seen from the previous quarterly report, Case 1 had a linear capillary function for the fracture blocks with 200 kPa as the maximum. The maximum capillary pressure values were 100, 50 and 0 kPa for Cases 2, 3 and 4, respectively.

6.2 RESULTS AND DISCUSSION

In Case 1 (Fig. 6.1), the saturations were not monotonically decreasing with depth. Based on the one-dimensional behavior such a monotonic behavior should be observed. One plausible reason is that the system is not in steady-state. Indeed, observing the fracture block parameters with time indicated that the pressures, temperatures and saturations were oscillating with time.
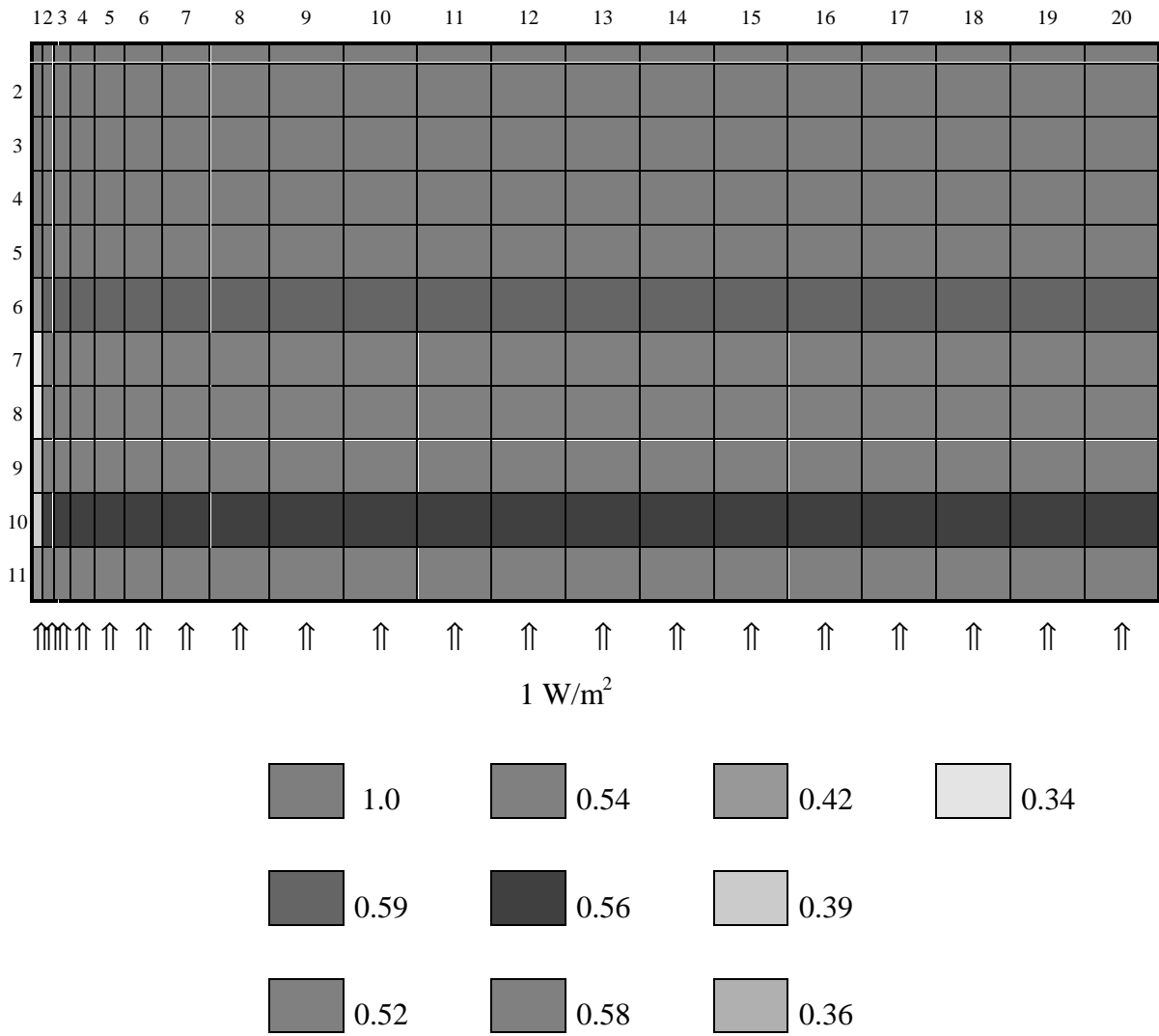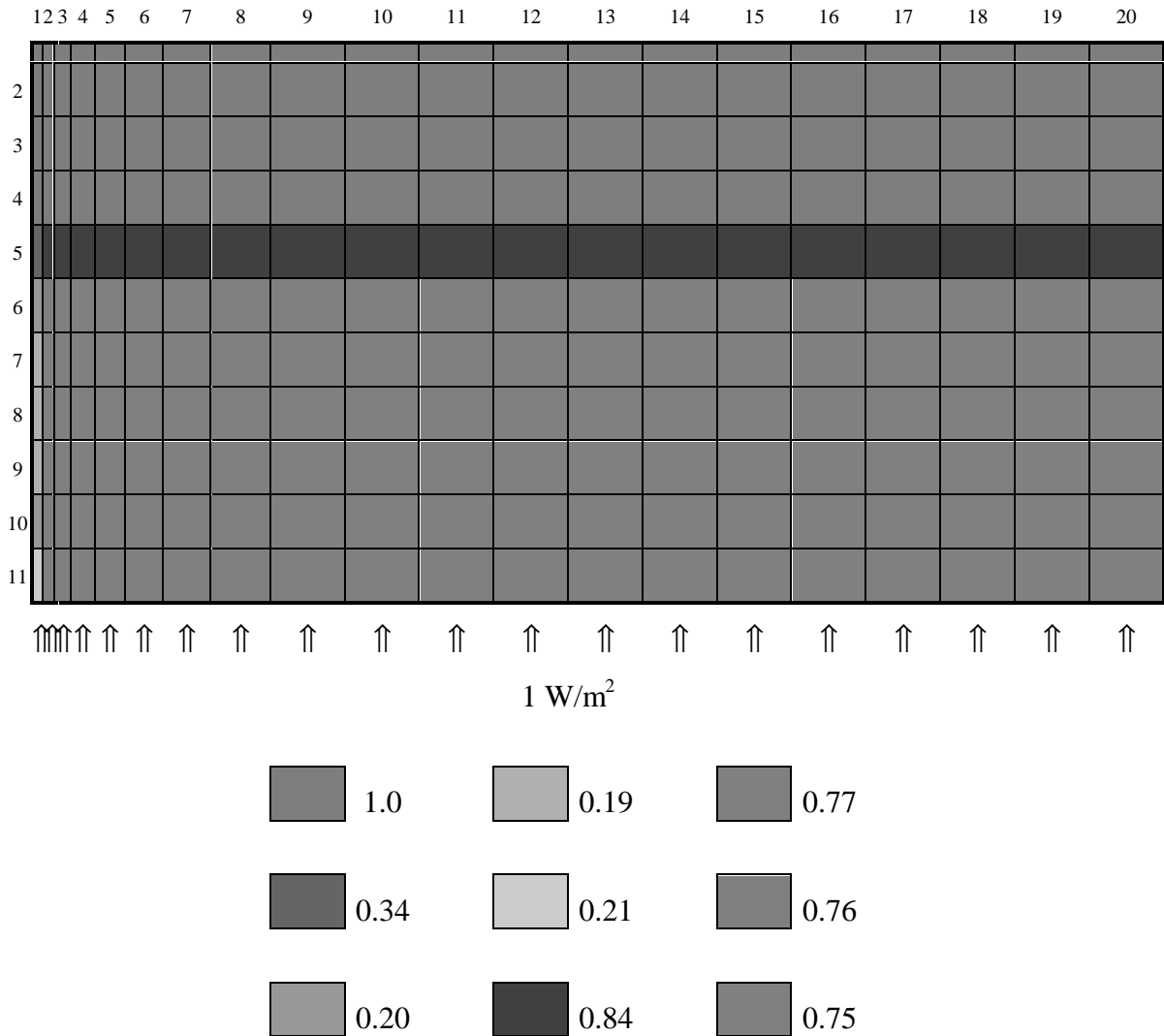
Figure 6.1 Water Saturation: Case 1.

Figure 6.2 Water Saturation: Case 2.

For Cases 2 to 4 (Figs. 6.2 -6.4) layers 1 to 4 were all liquid-filled. Lowering the capillary pressure in the fracture from 100 to 50 kPa results in a state where the steam prefers to be in the fracture. In fact, when we do not specify any capillary pressure function in the fracture, the matrix is liquid-filled and the steam resides in the fracture.

The results obtained by using five-point differencing as compared to that for nine-point are different. One difference is that, for Case 1 (5-pt. differencing) a steady state solution was not obtained. Also the location of the liquid-two-phase interface and the saturation values are different.

The same general behavior, however, is observed from the results of the five-point and the nine-point differencing scenarios. Capillary forces do influence the fluid flow between the

23

fracture and the adjacent matrix. In Case 2, the capillary pressure in the fracture was high. Therefore, more fluid is sucked into the crevices and this explains the existence of the two phases in the fracture. As we lower the maximum capillary pressure, less of the liquid is retained. This accounts for the decrease in water saturation and the development of steam-filled fracture blocks.
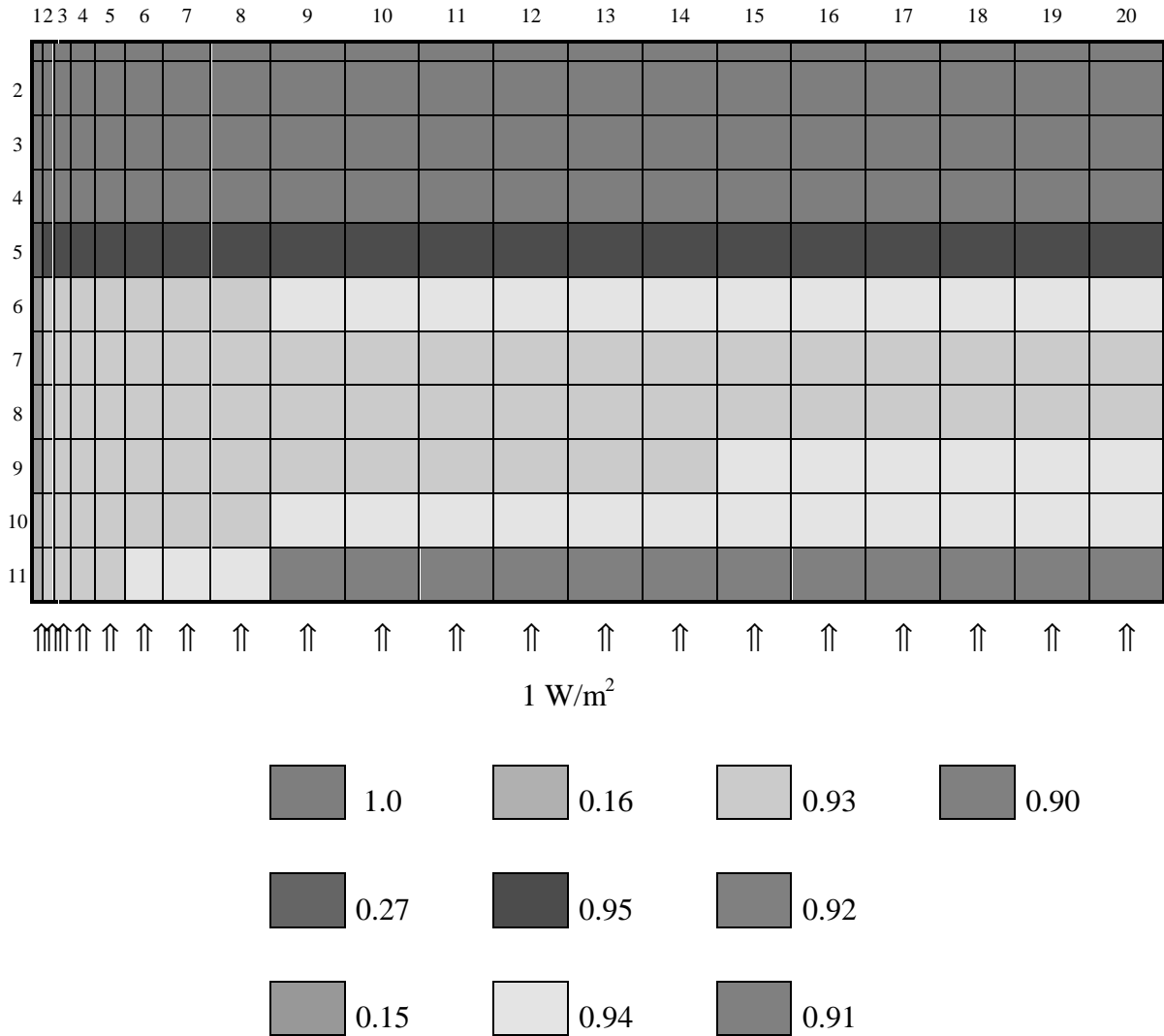

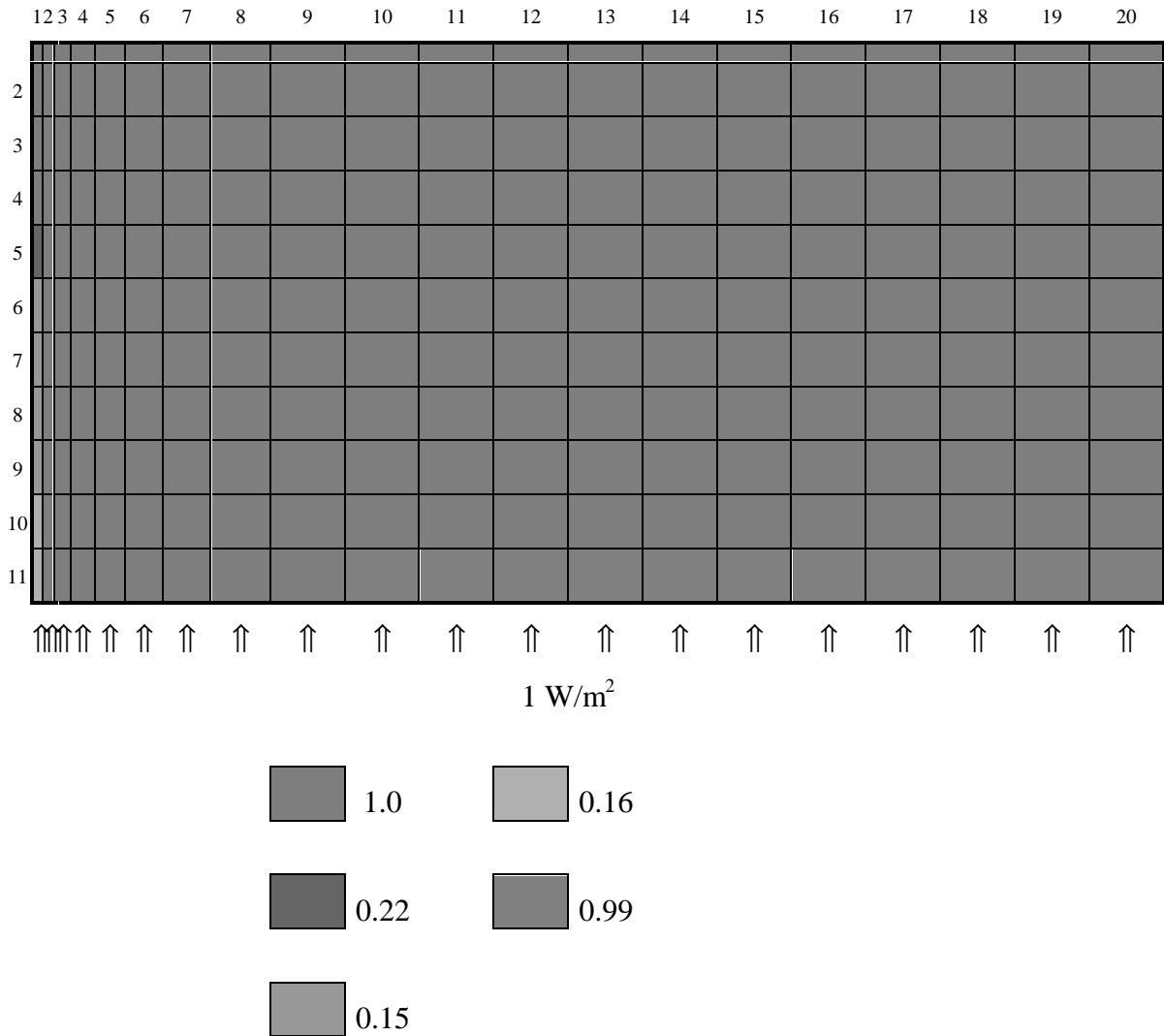*Figure 6.3 Water Saturation: Case 3.*

Figure 6.4 Water Saturation: Case 4.

4.3 SUMMARY

Simulation runs using five-point differencing were performed. Comparing these results to those obtained using nine-point differencing shows that the calculated saturation distributions are not the same. In spite of this, the same conclusion can be derived regarding the effect of capillary pressure. However, we still have to look further into the effects of capillarity on fluid flow.

Because of the different results obtained when two different differencing schemes were employed, it is desirable to duplicate the experimental results for the heat pipe experiment.

This will determine which differencing scheme will be suitable for the particular system under investigation.

7 MODELING OF GEOTHERMAL RESERVOIRS CONSTRAINED TO INJECTION RETURN DATA

This project is being conducted by Research Assistant Ma. Michelle Sullera and Prof. Roland Horne. It aims to deduce injection return mechanisms and flow paths from correlations between producer chloride concentration and injection operating parameters (flow rate and injection chloride).

7.1 BACKGROUND

We have taken a general approach to the problem in three steps. The first step is to find a correlation between chloride concentrations in production wells and injection rates. The second step is deduce mechanisms, consistent with the correlation obtained previously, by which injectate returns to the reservoir and is reproduced. The final step will be to verify the accuracy of these mechanisms by incorporating them into a simulation model of the reservoir and generating history matches.

So far, production and injection data from Palinpinon-I geothermal field in the Philippines have been analyzed; specifically, two linear models were used to correlate production chloride concentration and injection rates:

CORRELATION 1

$$Cl_p = a_0 + a_1 Q_{I1} + a_2 Q_{I2} + a_3 Q_{I3} + \ldots \quad \ldots + a_n Q_{In} \tag{7.1}$$

CORRELATION 2

$$Cl_p = a_0 + a_1 Q_{I1} + a_2 Q_{I2} + a_3 Q_{I3} + \ldots \quad \ldots + a_n Q_{In} + bt \tag{7.2}$$

where Cl_p = chloride concentration in production well, P

Q_{In} = mass flow rate to injection well, In

a_n = linear coefficient of well In

a_0 = a constant associated with local chloride concentration

t = time

Previous results have shown that Correlation 2 fits the data better than Correlation 1; however, Correlation 2 was also shown to have a poor predictive capacity.

7.2 LATEST RESULTS AND DISCUSSION

It was suggested that incorporation of more data into Correlation 2 could improve its predicting capacity. In the absence of additional data from the same field (Palinpinon I), data from a different field was used instead to test correlations 1 and 2. The new set of data came from the geothermal field in Dixie Valley, Nevada, and have been provided to us by the courtesy of Oxbow Geothermal, Inc. In addition to production chloride concentration and injection rate, injectate chloride concentration data was also available from Dixie Valley. This made it possible to test two additional linear models.

CORRELATION 3

$$Cl_p = a_0 + a_1 Q_{I1} Cl_{I1} + a_2 Q_{I2} Cl_{I2} + a_3 Q_{I3} Cl_{I3} + \dots \quad \dots + a_n Q_{In} Cl_{In} \tag{7.3}$$

CORRELATION 4

$$Cl_p = a_0 + a_1 Q_{I1} Cl_{I1} + a_2 Q_{I2} Cl_{I2} + a_3 Q_{I3} Cl_{I3} + \dots \quad \dots + a_n Q_{In} Cl_{In} + bt \tag{7.4}$$

The additional parameter Cl_{In} refers to the chloride concentration of the fluid being injected to injection well In.

Values of the linear coefficients in Eqns. (7.1), (7.2), (7.3), and (7.4) were calculated using Microsoft Excel's regression analysis tool and the predicted values of chloride were plotted against actual data. Typical results for one of the production wells are shown in Figs. (7.1), (7.2), (7.3), and (7.4).
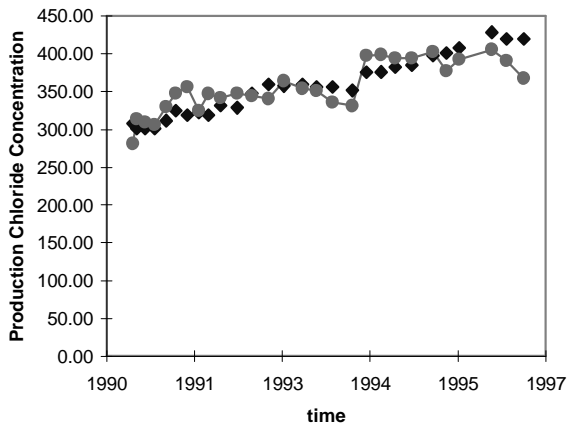
Regression Statistics	
Multiple R	0.846384713
R Square	0.716367083
Adjusted R Square	0.596942696
Standard Error	24.96698404
Observations	28

	Coefficients
a_0	172.3266278
a_1	0.001873331
a_2	-0.000674837
a_3	-0.001138023
a_4	-0.000163113
a_5	-0.000860807
a_6	0.004493928
a_7	-0.003592451
a_8	0.000673401

Fig. 7.1 Actual vs. predicted chloride concentration using Correlation 1.
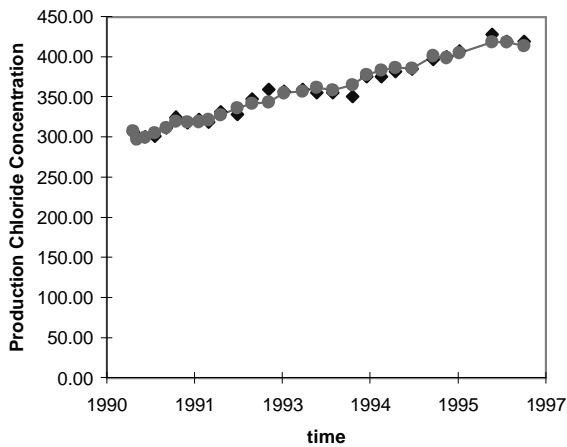
Regression Statistics	
Multiple R	0.988986284
R Square	0.978093871
Adjusted R Square	0.967140806
Standard Error	7.128713108
Observations	28

	Coefficients
a_0	271.5967735
a_1	0.000399139
a_2	3.88698E-05
a_3	-0.001236295
a_4	9.76142E-07
a_5	-0.000142197
a_6	0.00206649
a_7	-0.000723647
a_8	-0.000327493
b	19.04273981

Fig. 7.2 Actual vs. predicted chloride concentration using Correlation 2.
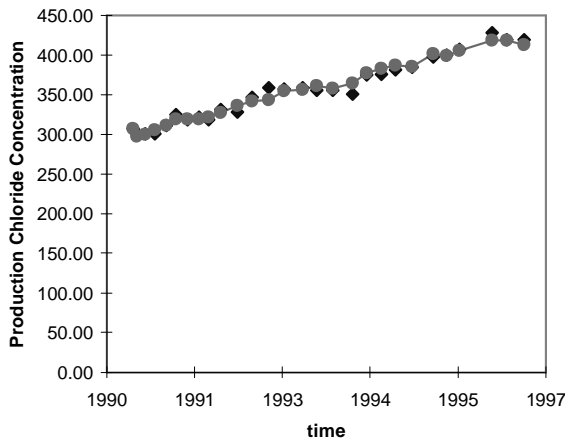
Regression Statistics	
Multiple R	0.988992245
R Square	0.978105661
Adjusted R Square	0.967158491
Standard Error	7.126794495
Observations	28

	Coefficients
a_0	276.7131374
a_1	7.29197E-07
a_2	3.29672E-08
a_3	-2.44222E-06
a_4	4.79593E-08
a_5	-3.22666E-07
a_6	4.39393E-06
a_7	-1.32695E-06
a_8	-7.46547E-07
b	17.73870441

Fig. 7.3 Actual vs. predicted chloride concentration using Correlation 3.
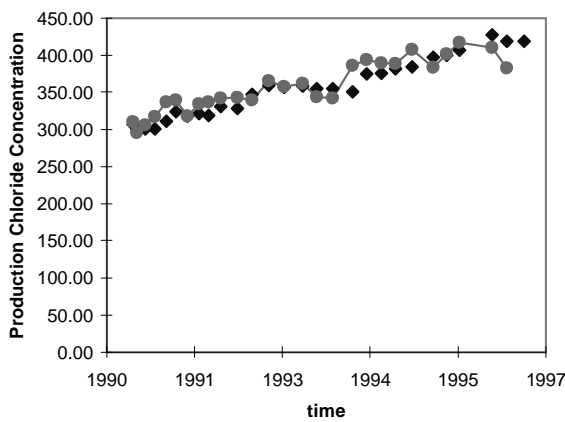
Regression Statistics	
Multiple R	0.936549186
R Square	0.877124378
Adjusted R Square	0.825387274
Standard Error	16.43314293
Observations	28

	Coefficients
a_0	181.401406
a_1	3.73811E-06
a_2	3.71788E-07
a_3	-3.08959E-06
a_4	-4.69869E-07
a_5	-4.47093E-07
a_6	7.97848E-06
a_7	-4.06998E-06
a_8	-4.32323E-07

Fig. 7.4 Actual vs. predicted chloride concentration using Correlation 4.

As with the Palinpinon data, some of the coefficients had negative values. This would imply that the operation of injection wells corresponding to those negative coefficients can actually lessen the percentage of injectate being produced. One plausible explanation is that the injectors with negative coefficients could be diverting the flow from the other injectors away from the production well. Unfortunately, an alternate explanation is that the linear model is not appropriately representing the data.

30

Based on values of the multiple regression coefficient, Correlations 2 and 3 fit the data best (R is closest to 1). Both correlations include a linear term in time.

To test how well Correlation 2 can predict chloride concentrations, only the portion of the data set spanning 1990 and 1994 were used to calculate the coefficients and chloride concentrations for the succeeding two years were predicted. Results plotted in Fig. 7.5 show the model to underestimate the chloride concentration for the succeeding years by 9.2%, maximum. Examination of the data revealed that one of the injection wells was operating between 1990 and 1994 but ceased injecting in 1995; thus, the contribution of this injection well has not been properly accounted for by just using the early portion of the data set and this explains the resulting underprediction. Including additional data from 1994 to late-1995 improved Correlation 2's predicting capacity (Fig. 7.6), resulting in a maximum of 4.6% difference between the predicted and the recorded chloride concentration.
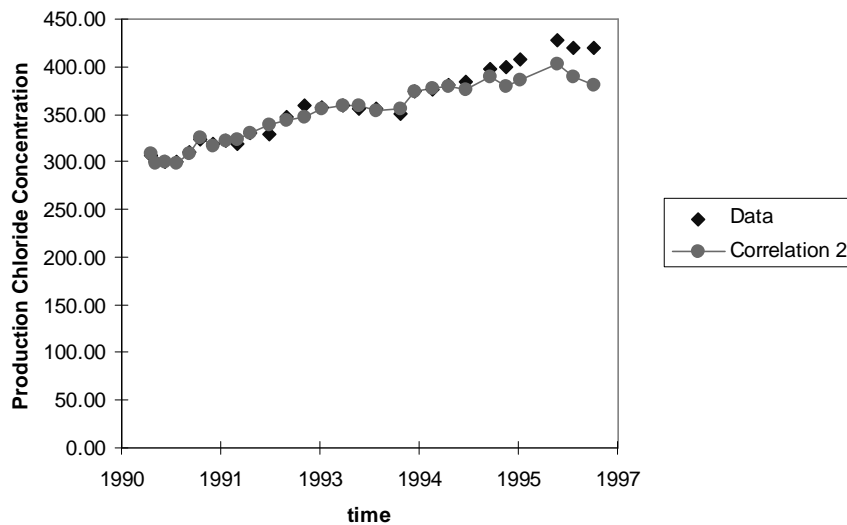

Fig. 7.5 Actual vs. predicted chloride concentration using Correlation 2 and data from 1990 to 1994.
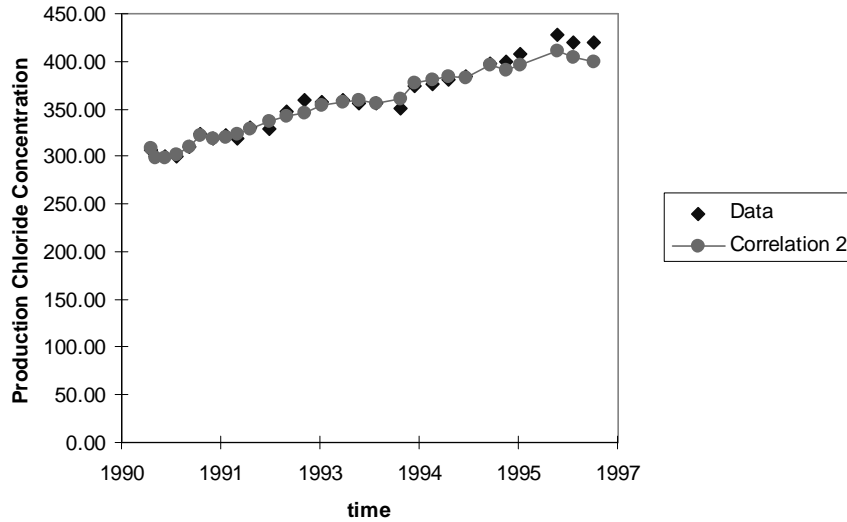
Fig. 7.6 Actual vs. predicted chloride concentration using Correlation 2 and data from 1990 to late-1995.

7.3 FUTURE PLANS

Correlations 2 and 3 gave good matches over the range of data where the coefficients were calculated from; moreover, Correlation 2's predicting capacity was shown to improve with more data. As more data are made available, the predicting capacities of Correlation 2 and 3 will be assessed further.

It was mentioned earlier that the magnitude of the linear coefficients is related to the degree of connectivity of the production well with the injection well corresponding to each of those coefficients. In addition, regression analysis provides tests which give the level of significance of the relationship between an independent variable (in this case injection rates, injectate chloride concentration, and time) and the dependent variable, production chloride concentration. These tests will be applied to data sets from both Palinpinon-I and Dixie Valley and based on the results individual linear models involving only the more significant independent variables may be developed for each of the production wells.

After arriving at a satisfactory correlation, we plan to incorporate it within a reservoir model and generate production history matches to test its accuracy. We have recently obtained TOUGH2 and TETRAD simulation models of Dixie Valley geothermal field from ESRI for this purpose.

REFERENCES

Akin, S., Demiral, B., and Okandan, E., "A Novel Method of Porosity Measurement Utilizing Computer Tomography", *In Situ*, 20(4),347-365 (1996)

Barton, C. A., S. Hickman, R. Morin, M. D. Zoback, T. Finkbeiner, J. Sass, and D. Benoit, "Fracture Permeability and its Relationship to In-situ Stress in the Dixie Valley, Nevada, Geothermal Reservoir", *Proceedings*, 22nd Workshop on Geothermal Reservoir Engineering, Stanford University, Jan. 1997, Stanford California.

Bodvarsson, G. S., and C. F. Tsang, "Injection and Thermal Breakthrough in Fractured Geothermal Reservoirs", *J. Geophysical Research*, vol. 87, no. B2, pgs. 1031-1048, Feb. 1982

Bodvarsson, G. S., K. Pruess, and M. J. O'Sullivan, "Injection and Energy Recovery in Fractured Geothermal Reservoirs", *Soc. Petroleum Engrs. J.* 25, pgs. 303-312, 1985

Bonner, B.P., J.J. Roberts and D. J.Schnelbert, "X-Ray Evidence for Capillary Pressure Driven Flow in Preserved Core from Geysers", *Proceedings*, 22nd Workshop on Geothermal Reservoir Engineering, Stanford University, January 27-29, 1997

Carslaw, H. S., and J. C. Jaeger, Conduction of Heat in Solids, 2nd ed., Clarendon, Oxford, 1959.

Gringarten, A. C., P. A. Witherspoon, and Y. Ohnishi, "Theory of Heat Extraction from Fractured Hot Dry Rock", *J. Geophysical Research*, vol. 90, no. 8, March, 1975.

Huang, Y., P. S. Ringrose and K. S. Sorbie, "X-ray Imaging of Waterflood Fluid Saturation in Heterogeneous Rock Slabs", SPE 30000, pp. 483-495

Johns, R.A., "Diffusion and Dispersion of Solute in a Variable Aperture Fracture", 1991, Ph. D dissertation, Stanford University

Macovski, A. (1983), "Medical Imaging System",Prentice Hall

Melrose, J. C., Dixon, J. R. and Mallinson, J. E. Comparison of Different Techniques for Obtaining Capillary Pressure Data in the Low-Saturation Region.*SPE 22690.* (1991).

Pruess, K., "Heat Transfer in Fractured Geothermal Reservoirs with Boiling", *Water Resources Res.*, 19, 201-208, 1983.

Robinson, B. A., and P. Kruger, "*Pre-test Estimates of Temperature Decline for the LANL Fenton Hill Long-term Flow Test*", Geothermal Resources Council Transactions, vol. 16, Oct. 1992, San Diego, California.

Sta. Maria, R. and Pingol, A. "Simulating the Effects of Adsorption and Capillary Forces in Geothermal Reservoirs",*Proc.* Stanford Geothermal Workshop **18**, (1996), 165-173.

Satik, C., 1994, "Studies In Vapor-Liquid Flow In Porous Media", *Ph.D. Thesis,* University of Southern California, Los Angeles, CA

Satik, C., 1997, "Experiments of Boiling in Porous Media", Proc. of 22nd Stanford Workshop on Geothermal Reservoir Engineering, Stanford, CA

Satik, C. and Yortsos, Y.C., 1996, "A Pore Network Study of Bubble Growth in Porous Media Driven By Heat Transfer", *J. Heat Transfer,* **118**